Renormalization of a Landau-Ginzburg-Wilson theory of microemulsion

Y. Levin
Department of Physics, University of California, Berkeley, California 94720

C. J. Mundy
Department of Chemistry, University of California, Berkeley, California 94720

K. A. Dawson
Department of Chemistry, University of California, Berkeley, California 94720
and Department of Chemistry, University College Dublin, Belfield, Dublin 4, Ireland

(Received 27 August 1991)

We study the effects of fluctuations on the mean-field phase diagram of a Landau-Ginzburg-Wilson (LGW) action of the form $H=\frac{1}{2}\int_{\mathbf{q}}|\varphi_{\mathbf{q}}|^2(\mathbf{q}^4+b\mathbf{q}^2+c)d\mathbf{q}+\lambda/4!\int_{\mathbf{q}}\varphi_{\mathbf{q}_1}\varphi_{\mathbf{q}_2}\varphi_{\mathbf{q}_3}\varphi_{\mathbf{q}_4}\delta(\mathbf{q}_1+\mathbf{q}_2+\mathbf{q}_3+\mathbf{q}_4)$, where b may be positive or negative. In the latter case the inclusion of fluctuations may produce large quantitative and qualitative effects in the phases and the transitions between them. The renormalization is accomplished by resummation to all orders of two classes of diagrams and is reminiscent of a calculation earlier described by Brazovskii (Zh. Eksp. Teor. Fiz. **68**, 175 (1975) [Sov. Phys.—JETP **41**, 85 (1975)]). Since the LGW theory (with $b<0$) may be extracted from an isotropic frustrated-lattice model of microemulsion it is possible to compare the predictions of the present study with earlier Monte Carlo simulations of the Ising model. It is therefore also possible to describe the correlation functions in the disordered phase, which had earlier been identified as the bicontinuous phase of the microemulsion model. In particular, strong renormalizations of the two length scales d and ξ originally introduced by Teubner and Strey [J. Chem. Phys. **87**, 3195 (1987)] to describe the bicontinuous-microemulsion phase are derived. In addition renormalizations of the surface energies are derived and discussed in the context of bicontinuous microemulsion.

PACS number(s): 82.70.Kj, 64.60.Ak, 64.60.Cn, 68.45.Gd

I. INTRODUCTION

There are a number of physical systems that are described by a Landau-Ginzburg-Wilson (LGW) Hamiltonian where the signs of the gradient and squared-gradient terms are, respectively, negative and positive. This situation is quite different from the familiar LGW theory of the nearest-neighbor Ising model and, it may be shown, reflects the presence of spatial frustration in the underlying lattice model. Thus, ordering problems in alloys, frustration in the exchange interactions of spin models [1], and latterly, systems containing oil, water and surfactant all may be discussed with such a LGW Hamiltonian [2]. Our discussion will focus on the latter, but the calculations we describe apply equally well to these other situations.

The thermodynamic structure of the systems composed of oil, water, and amphiphile presents a fascinating theoretical and experimental problem. There have been numerous experiments in this area, including thorough studies of phase diagrams, small-angle-neutron-scattering (SANS) experiments, and measurements of the interfacial tensions [3]. These have led to the development of our understanding of the complex structure of microemulsion. For example, the SANS measured structure factor in the bicontinuous microemulsion phase has been shown to have a maximum at long but not diverging length scales. It has been argued that this implies the presence of some long-range order on "mesoscopic" length scales within the disordered phase. This phenomenon has been explored by Teubner and Strey [4], who proposed a fit to the scattering data which implies the presence of two length scales. Thus, from Orstein-Zernike theory we expect that the correlation function in a disordered fluid to decay as

$$g(\mathbf{r}-\mathbf{r}')\approx\frac{e^{-|r-r'|/\xi}}{|\mathbf{r}-\mathbf{r}'|} \tag{1.1}$$

with ξ being the fundamental length scale. Teubner and Strey found a remarkably accurate fit to experiments on bicontinuous microemulsion using the correlation function

$$g(\mathbf{r}-\mathbf{r}')\approx\frac{e^{-|r-r'|/\xi}}{|\mathbf{r}-\mathbf{r}'|}\sin\frac{2\pi|\mathbf{r}-\mathbf{r}'|}{d}\ . \tag{1.2}$$

Here, d may be interpreted as a new length scale describing the incipient periodic ordering. They related this to a Gaussian Hamiltonian that had gradient and squared-gradient terms of opposing signs, an insight that also elucidated the relevance of the lattice models to the study of microemulsion.

Quite a bit may be said about d and ξ. From experiments performed by Chen *et al.* [3], one finds that the ratio of d/ξ typically lies in the range 2.6–4.5. Also, one can understand the evolution of d and ξ as a function of surfactant concentration [3].

The above experimental observations are signatures of what we call bicontinuous microemulsion. There are many other experimental observations that appear to be correlated with those described above. For example, numerous experiments have been carried out to measure interfacial tensions and the wetting behavior. One can show that these phenomena are also implicit in the LGW theory of the type discussed in the present paper [6].

However, we shall focus mainly on the phase diagram and correlation functions.

Numerous theoretical models have been devised to try to explain the experimental observations. One approach, first proposed by Widom [4], consists of constructing a lattice model for the oil-water-amphiphile solution. The resulting model consists of + and − spins placed on the cubic lattice having nearest-, next-nearest, and diagonal-neighbor interactions. The Hamiltonian can be conveniently written using lattice difference operators [5]:

$$H=\tfrac{1}{2}\sum_{\mathbf{n}}\sigma_{\mathbf{n}}L_{\mathbf{n}}\sigma_{\mathbf{n}}\ ,\quad L_{\mathbf{n}}=a_4\Delta_{\mathbf{n}}^4+a_2\Delta_{\mathbf{n}}^2+a_0\ , \tag{1.3}$$

$$\Delta_x^2 f_x=f_{x+1}+f_{x-1}-2f_x\ ,\quad x=0,\pm1,\pm2,\ldots\ , \tag{1.4}$$

$$a_4=-m,\quad a_2=-(j+12m),\quad a_0=-6(j+5m)\ , \tag{1.5}$$

where j is related to the chemical potential of the amphiphile, relative to that of oil and water, and m is related to the length of the amphiphile chain. This Hamiltonian was earlier analyzed within mean-field theory [5] and a complete phase diagram in terms of the microscopic coupling constants j and m was derived, in less detail, by Monte Carlo simulation [7].

All of the bicontinuous microemulsion phenomena, including interfacial tensions, and the form of the structure factor, appear to be captured in an extended model [6]. However, when microscopic parameters for microemulsion extracted from the mean-field phase diagram are inserted into the equations for d and ξ, the results follow neither the evolution given by experiment, nor by Monte-Carlo simulations [2]. The reason for the failure of these formulas is that fluctuations have been neglected.

Actually, it is also of interest to study the amphiphile-amphiphile (lipid-lipid) correlation function. However, for technical reasons, which will be discussed in Appendix C, fluctuations are more difficult to treat in this case so we choose not to include it in our present study.

Here we present a systematic analytical treatment of fluctuations. For the solvent correlation function this is accomplished by constructing a coarse-grained LGW Hamiltonian corresponding to the microscopic Hamiltonian (1.3). Even though the mean-field treatment of the lattice model fails in accounting for fluctuations properly, we believe that the underlying relationships between the microscopic variables and macroscopic properties which are obtained in the formulation of the lattice model are correct. This conclusion can be justified qualitatively by examining the Monte Carlo simulation of the lattice model [7]. In any case the results of the Monte Carlo simulations are in effect the "exact" answer to the three-dimensional-lattice model.

Now if one compares the mean-field phase diagram with the Monte Carlo phase diagram one sees remarkable similarities, except that there is a shift of the order-disorder transition temperatures by 200% in regions of the phase diagram where spatially inhomogeneous phases are present [7]. Also, in these same regions the order of the transition is changed from the mean-field prediction of second-order to a weak first-order transition [7]. It was previously shown how this change could be studied within the renormalization group [8]. There, it was pointed out that the renormalization-group flow was confined to that region of parameter space were no fixed points were accessible, this resulting in a runaway trajectory. This is the usual scenario for the weak fluctuation-induced first-order transition. However, such an analysis gives no information on the properties of the phases or details of the transformations. In the present calculation, the fluctuation effects are explicitly taken into account by summing up to all orders the leading classes of diagrams. Scattering data and the evolution of d and ξ are computed and compared to the Monte Carlo simulation. The explicit equation for the first-order phase-separation line is found in terms of microscopic parameters.

II. THE HAMILTONIAN

We begin our study by constructing an effective LGW Hamiltonian [8]. To do this we perform a Hubbard transformation on the partition function of the Hamiltonian (1.3). The result of this transformation is

$$Z=\sum_{\{\sigma_n\}}e^{-H}=\int D\varphi_{\mathbf{n}}e^{-H(\varphi_n)}\ , \tag{2.1}$$

$$D\varphi_n=\frac{1}{(\det L_n)^{1/2}}\prod_n\frac{d\varphi_n}{(2\pi)^{1/2}}\ , \tag{2.2}$$

$$H=-\tfrac{1}{2}\sum_{\mathbf{n}}\varphi_{\mathbf{n}}L_{\mathbf{n}}^{-1}\varphi_{\mathbf{n}}-\sum_{\mathbf{n}}\ln(2\cosh\varphi_{\mathbf{n}})\ . \tag{2.3}$$

The LGW Hamiltonian is constructed by expanding the last term in the equation and keeping only the terms up to quartic order, since typically, all of the higher powers will be irrelevant to the study of near critical behavior of the theory. Transforming to Fourier space we see that the coefficient of the quadratic term is $-L_q^{-1}-1$. We therefore define

$$K_q=L_q+1 \tag{2.4}$$

within the mean-field theory, the phase transition from the paramagnetic to the nonuniform phase with wave vector $\mathbf{q}_c$ occurs at $K_{q_c}=0$ and $\nabla K_{q_c}=0$ [5]. Thus, close to the transition line we can expand in powers of K_q to obtain

$$H=\tfrac{1}{2}\int_{\mathbf{q}}|\varphi_{\mathbf{q}}|^2K_{\mathbf{q}}d\mathbf{q}+\tfrac{1}{12}\int_{\mathbf{q}}\varphi_{\mathbf{q}_1}\varphi_{\mathbf{q}_2}\varphi_{\mathbf{q}_3}\varphi_{\mathbf{q}_4}\delta(\mathbf{q}_1+\mathbf{q}_2+\mathbf{q}_3+\mathbf{q}_4)\ . \tag{2.5}$$

The Hamiltonian (2.5) is a coarse-grained version of the original lattice-model Hamiltonian (1.3), and the coefficients b in Eq. (2.6) are very similar to coefficients a of Eq. (1.5).

In this paper we shall concentrate our attention on that region of the phase diagram in the vicinity of the Lifshitz point ($\mathbf{q}_c=\mathbf{0}$). In this region it is possible to expand K_q in the powers of $\mathbf{q}$ to obtain

$$K_{\mathbf{q}}=b_0+b_1\mathbf{q}^2+b_3\mathbf{q}^4+b_4\sum_{i=1}^{3}q_i^4\ , \tag{2.6}$$

where

$$b_0 = 1 - 6(j + 5m) , \tag{2.7}$$

$$b_1 = (j + 12m) , \tag{2.8}$$

$$b_3 = -m , \tag{2.9}$$

$$b_4 = -\tfrac{1}{12}(j + 12m) , \tag{2.10}$$

and $i = 1$, 2, and 3 denotes the x, y, and z directions, respectively. It is worth pointing out that the resulting form of the LGW Hamiltonian is believed to be the simplest possible for description of the bicontinuous phase and, therefore, in some sense is canonical. The scaling of the bare coupling constants with the microscopic energies and chemical potentials is an additional benefit of having begun with a lattice model.

Now the physical meaning of the term quadratic in momentum is evidently just a surface energy. We also note that the coefficient b, the effective bare tension, contains both an interaction term (m) and the relative chemical potential (j) [2,5]. Therefore the bare tension may be chosen by adjusting molecular structure and concentrations independently. In this regard it is important to maintain the picture of the interface as one that is truly open to mass transfer, rather than a simple mechanical surface. The coefficient of the quartic term in momentum reflects both curvature and compression contributions, and will also serve to set the energy scale, while the φ^4 term is the leading effect of the excluded-volume interactions. Since near the Lifshitz point the cubic anisotropy is small, we may spherically average the last term in Eq. (2.6). Finally normalizing the quartic term of (2.6) to $\frac{1}{2}$ we have the effective action

$$H = \tfrac{1}{2}\int_{\mathbf{q}} |\varphi_{\mathbf{q}}|^2 (\mathbf{q}^4 + b\mathbf{q}^2 + c)\, d\mathbf{q} + \frac{\lambda}{4!}\int_{\mathbf{q}} \varphi_{\mathbf{q}_1}\varphi_{\mathbf{q}_2}\varphi_{\mathbf{q}_3}\varphi_{\mathbf{q}_4}\delta(\mathbf{q}_1 + \mathbf{q}_2 + \mathbf{q}_3 + \mathbf{q}_4) \tag{2.11}$$

and

$$b = \frac{-20(j + 12m)}{(j + 32m)} , \tag{2.12}$$

$$c = \frac{120(j + 5m) - 20}{(j + 32m)} , \tag{2.13}$$

$$\lambda = \frac{800}{(j + 32m)^2} . \tag{2.14}$$

We will use this action as a starting point for the analysis of the fluctuations in model (1.3).

III. ANALYSIS OF FLUCTUATIONS

There is an important observation that may be made immediately. In the region of parameter space where $b < 0$, K_q will attain its minimum on a surface $|\mathbf{q}| = q_c$ and, thus, the volume of fluctuations of the order parameter will be large. To make this observation more concrete we calculate the zeroth-order approximation of $\langle \varphi^2(\mathbf{r}) \rangle$:

$$\langle \varphi^2(\mathbf{r}) \rangle = \frac{1}{(2\pi)^3}\int d^3\mathbf{q} \frac{1}{\mathbf{q}^4 + b\mathbf{q}^2 + c} . \tag{3.1}$$

The integral may easily be performed using contour integration to give

$$\langle \varphi^2(\mathbf{r}) \rangle = \frac{1}{4\pi(2\sqrt{c} + b)^{1/2}} . \tag{3.2}$$

Thus in the region where $2\sqrt{c} \cong -b$ the theory will be fluctuation dominated. It is interesting to see how this is related to the phase-transition line predicted by the mean-field theory. This line is given by the equations $K_{q_c} = 0$ and $\nabla K_{q_c} = 0$, which implies that

$$c(j,m) - \frac{b(j,m)^2}{4} = 0 \tag{3.3}$$

for the region of parameter space where $b < 0$ (below $j + 12m = 0$, see Fig. 2), this reduces to $2\sqrt{c} = -b$, the region of large fluctuations in Eq. (3.2). It is thus not very surprising that in the region where the action (2.11) is the correct continuum approximation to the Hamiltonian (1.3), the mean-field theory fails completely. The situation is similar to that encountered by Brazovskii in a somewhat different context [9]. He was able to demonstrate that the large phase-space volume of fluctuations was sufficient to change the order of the phase transition. We will use an analysis similar to his to try to understand the effects of fluctuations in the more general action (2.11).

Before beginning, it may be worth discussing at a qualitative level the effects that we seek to describe. From the examination of the Monte Carlo simulations we note that within mean-field theory the order-disorder transition occurs at much too small values of the couplings j and m, that is, at too high a temperature [5,7]. As expected, at this mean-field transition the propagator (1.2) falls off as a power law and, normally, renormalization-group procedures would account well for the coupling between the independent modes via the quartic spin term, affecting only the exponent of the power law and causing correlations between fluctuations to fall off more rapidly. This is expected to be the case when there are many fluctuations of comparable energy. However, in this case the density of states of such comparable modes is so large that coupling between them causes much more rapid decay of correlations than at a critical point. In fact, one can view the interaction of these modes as producing a sort of screening, causing the renormalized constants to produce a finite correlation length, rather than a simple modification of the critical exponent. Paradoxically, the magnitude of the effect is so great that it may be studied perturbatively, rather than requiring the complete machinery of the renormalization group. This is because the renormalized second-order transition is shifted to zero temperature, the true transition occurring via a first-order transition, at which the correlation length remains finite.

We study the renormalization of the coupling constants within a modified Hartree approximation. The fully self-consistent equation for the self-energy is shown diagrammatically in Fig. 1 and may be written

$$-\Sigma(\mathbf{p})=\frac{\lambda}{2}\frac{1}{(2\pi)^3}\int G(\mathbf{q};\Sigma)d^3\mathbf{q}+\frac{\lambda^2}{6}\left[\frac{1}{(2\pi)^3}\right]^2\int G(\mathbf{q};\Sigma)G(\mathbf{k};\Sigma)G(\mathbf{p}-\mathbf{q}-\mathbf{k};\Sigma)d^3\mathbf{q}d^3\mathbf{k}+O(\lambda^3)\ , \tag{3.4}$$

$$G(\mathbf{q};\Sigma)=\frac{1}{\mathbf{q}^4+b\mathbf{q}^2+c-\Sigma(\mathbf{q})}\ . \tag{3.5}$$

This equation corresponds to the resummation of the most divergent diagrams of the theory. We note that our choice of normalizing the coefficient of $\mathbf{q}^4$ to $\frac{1}{2}$ is a calculational convenience and was not necessary. It is satisfactory if the coefficient of the quartic term in the expansion of $\Sigma(\mathbf{q})$ is small. Later we shall see that, typically, this is indeed the case.

The one-loop diagram, being momentum independent, will renormalize only the coefficient c, while the other diagrams will renormalize both the quadratic and quartic terms via the second and fourth derivatives of $\Sigma(\mathbf{q})$ in a Taylor expansion for small q. That one may neglect the higher powers of q that are generated by renormalization and truncation of the self-consistent series at low orders in the evaluation of $\Sigma''(0)$ and $\Sigma''''(0)$ is an assumption that is difficult to justify rigorously [9], though one can estimate the corrections by evaluation of one further order than that considered in the renormalization. However, on general grounds one can argue that the corrections are small. The interested reader should consult Appendix B for a discussion of this point.

Now the one-loop integral has been previously performed in Eq. (3.2). It is, however, more convenient to perform the two-loop integral in real-space:

$$\left[\frac{1}{(2\pi)^3}\right]^2\int G(\mathbf{q})G(\mathbf{k})G(\mathbf{p}-\mathbf{q}-\mathbf{k})d^3\mathbf{q}d^3\mathbf{k}$$
$$=\int e^{i\mathbf{p}\cdot\mathbf{r}}G^3(\mathbf{r})d^3\mathbf{r}\ . \tag{3.6}$$

$G(\mathbf{r})$ is just a two-point function $\langle\varphi(0)\varphi(\mathbf{r})\rangle$ that can easily be obtained by contour integration to give

$$G(\mathbf{r})=K\frac{e^{-r/\xi}}{r}\sin\left[\frac{2\pi}{d}r\right]\ , \tag{3.7}$$

where

$$K=\frac{1}{2\pi(4c-b^2)^{1/2}}\ , \tag{3.8}$$

$$\frac{1}{\xi}=\left[\frac{\sqrt{c}}{2}+\frac{b}{4}\right]^{1/2}\ , \tag{3.9}$$

$$\frac{2\pi}{d}=\left[\frac{\sqrt{c}}{2}-\frac{b}{4}\right]^{1/2}\ . \tag{3.10}$$

The renormalized c_r and b_r are given by

$$c_r=c-\Sigma(0)\ , \tag{3.11}$$

$$b_r=b-\tfrac{1}{2}\Sigma''(0)\ . \tag{3.12}$$

Here the prime stands for differentiation with respect to q. Inserting the above results into the self-consistent Eq. (3.4) we obtain

$$b_r=b-\frac{\lambda^2}{4\pi^2(xy)^{3/2}}\left[\frac{(xy)^{1/2}}{(9x+y)^2}-\frac{(xy)^{1/2}}{81(x+y)^2}\right]\ , \tag{3.13}$$

$$c_r=c+\frac{\lambda}{8\pi\sqrt{x}}+\frac{\lambda^2}{48\pi^2(xy)^{3/2}}\left[3\cot^{-1}3\left[\frac{x}{y}\right]^{1/2}-\cot^{-1}\left[\frac{x}{y}\right]^{1/2}\right]\ , \tag{3.14}$$

where

$$x=2\sqrt{c_r}+b_r\ , \tag{3.15}$$

$$y=2\sqrt{c_r}-b_r\ , \tag{3.16}$$

and b and c are the bare parameters given by Eqs. (2.12) and (2.13). Note that b_r has a status of a renormalized surface tension, measured relative to the curvature contribution. Also, in the results presented here the magnitude of the fourth derivative given by

$$\frac{1}{4!}\Sigma''''(0)=\frac{\lambda^2\pi K^3}{9}\left\{\frac{3}{4(a^2+b^2)^4}\sin\left[8\tan^{-1}\left[\frac{b}{a}\right]\right]-\frac{1}{4(a^2+9b^2)^4}\sin\left[8\tan^{-1}\left[\frac{3b}{a}\right]\right]\right\}\approx 10^{-3} \tag{3.17}$$

$[a=3/\xi,\ b=2\pi/d$, and K is given by Eq. (3.8)] is typically very much smaller than the renormalizations of the other energies. We can solve these nonlinear equations numerically for any given choice of bare couplings, b and c. One interesting choice [5,7] is to solve the equations along the ray $j+10m=0$. The significance of this ray stems from the observation that, along it, the amount of work required to insert an amphiphile between oil and

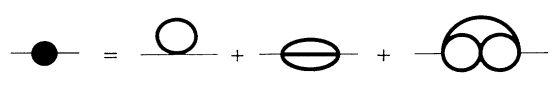

FIG. 1. The self-consistent equation for the self-energy in the modified Hartree approximation. Here the bold lines denote the renormalized propagator, and the filled circle is the self-energy. The first two diagrams have been evaluated in Sec. III. The final one [$O(\lambda^3)$] is discussed in Appendix B.

water is zero [2,5,7]. This ray also passes near the mean-field Lifshitz point (Fig. 2). The results are plotted as d and ξ and d/ξ (Figs. 3, 4, and 5) given by Eqs. (3.9) and (3.10) versus j along the ray. We may compare this evolution of d and ξ to that obtained within mean-field theory (Figs. 6 and 7). We see that the two are quite distinct, which is hardly surprising since, as we shall see in Sec. IV, the renormalization actually removes the second-order phase-transition predicted by mean-field theory. In fact, the variation of d and ξ as a function of j and at fixed m is more meaningful in the interpretation of the Hamiltonian as a microemulsion model. By considering the transcription from coupling to solution-model constants [4,5],

$$\Delta\mu = -\tfrac{5}{2}\kappa + j \ , \tag{3.18}$$

$$m = -\frac{\kappa}{4} \ , \tag{3.19}$$

one sees that this choice amounts to a fixed bending energy of the amphiphilic film (κ) and a decreasing amphiphile concentration ($\Delta\mu$). Evidently d should increase, reflecting the increase in domain size. The mean-field theory of this is qualitatively correct, while the renormalized theory agrees qualitatively, with fair quantitative agreement. As an example (Fig. 8) we consider the cut $m = -0.048$ for j between 0.5 and 0.66, a line that passes close to the renormalized Lifshitz region. The values of d increase and, in principle, diverge as one crosses the Lifshitz point. The Monte Carlo values of $m = -0.11$, and j varying between 0.65 and 0.95 corresponding to a cut close to the Monte-Carlo Lifshitz point, are presented in Fig. 9 for comparison. Though there is a fair amount of scatter in the points reflecting both statistical fluctuations and sensitivity to fitting for small and large values

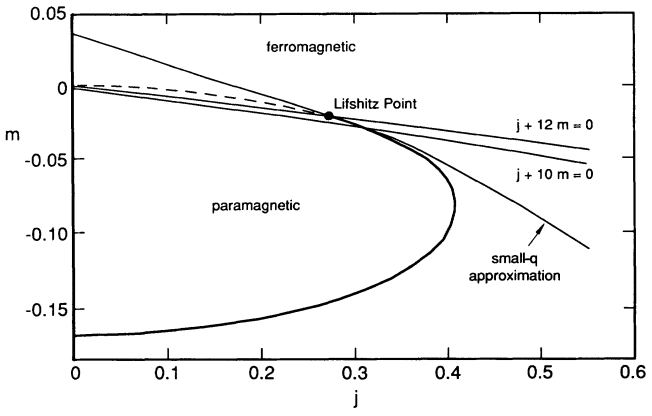

FIG. 2. The mean-field capped ellipse showing the phase transitions between the paramagnetic, ferromagnetic, and modulated phases. The intersection of the $j+12m=0$ line with the ellipse defines a Lifshitz point. Above this line the phase is ferromagnetic, $q_c=0$; below there are periodically modulated phases, $q_c>0$. The dashed line corresponds to the disorder line, below which the correlation function behaves as in Eq. (1.2), and above which the correlation function behaves as in Eq. (1.1). The hyperbola is the small-q approximation to the mean-field ellipse. As is expected it completely coincides with the ellipse near the Lifshitz point and overlaps with the disorder line.

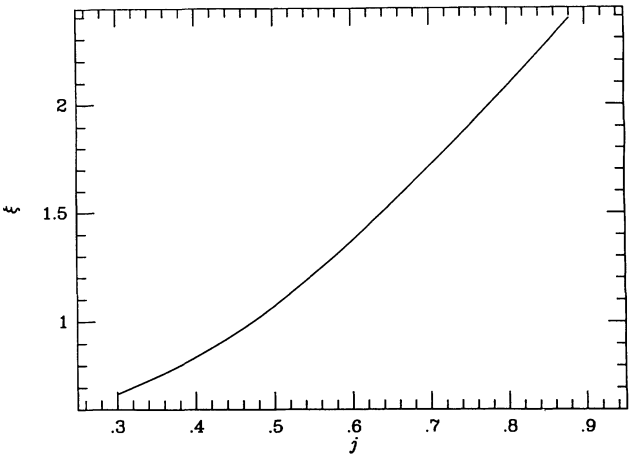

FIG. 3. The renormalized ξ along the $j+10m=0$ ray.

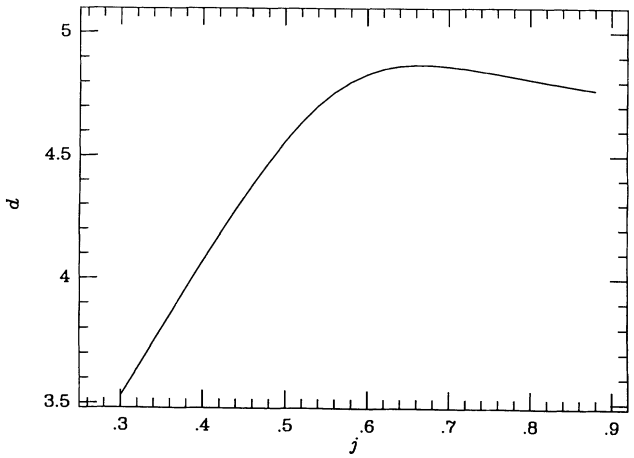

FIG. 4. The renormalized d along the $j+10m=0$ ray.

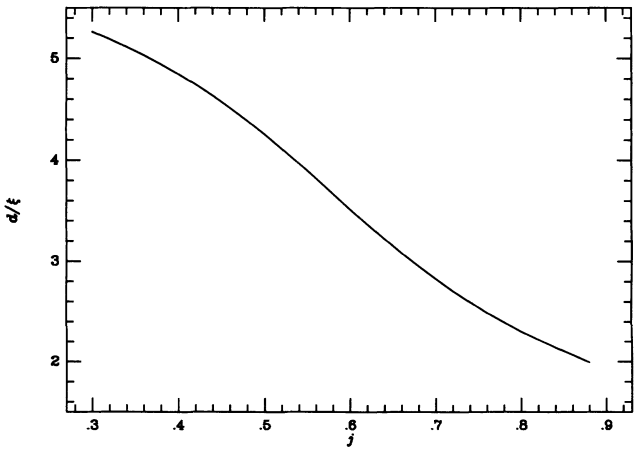

FIG. 5. The renormalized d/ξ along the $j+10m=0$ ray. These values are in reasonable agreement with experiment.

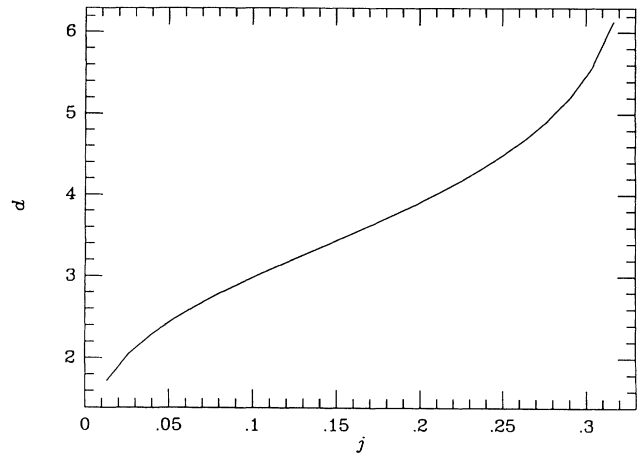

FIG. 6. The mean field d along the $j+10m=0$ ray. The precipitous rise in both d and ξ (see Fig. 5) is a consequence of the mean-field critical transition. Mean-field theory cannot, therefore, be applied to larger values of j.

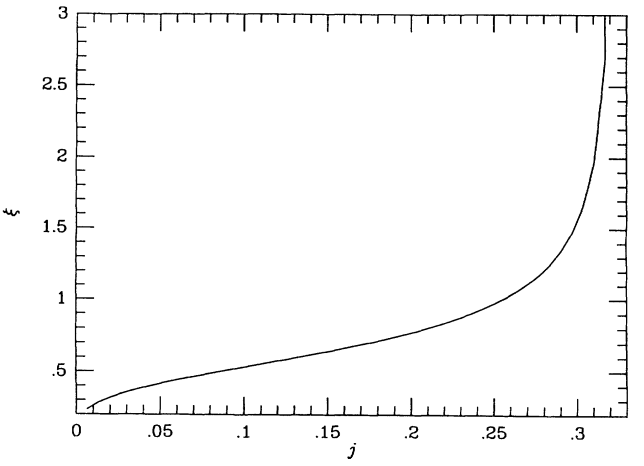

FIG. 7. The mean field ξ along the $j+10m=0$ ray. See also caption to Fig. 5.

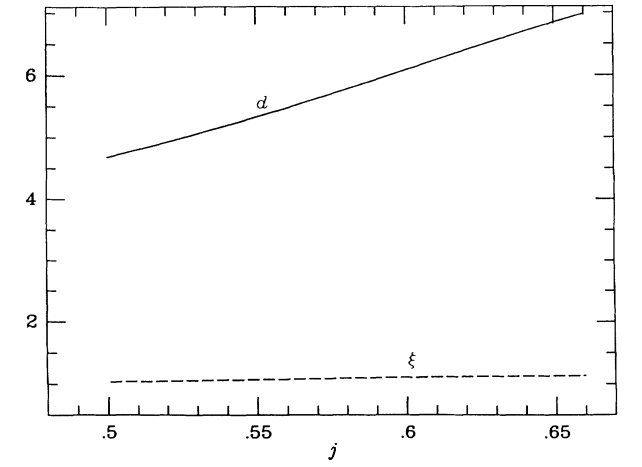

FIG. 8. The renormalized d and ξ as a function of j with m held at a constant value of -0.048. This ray passes close to the predicted renormalized Lifshitz point.

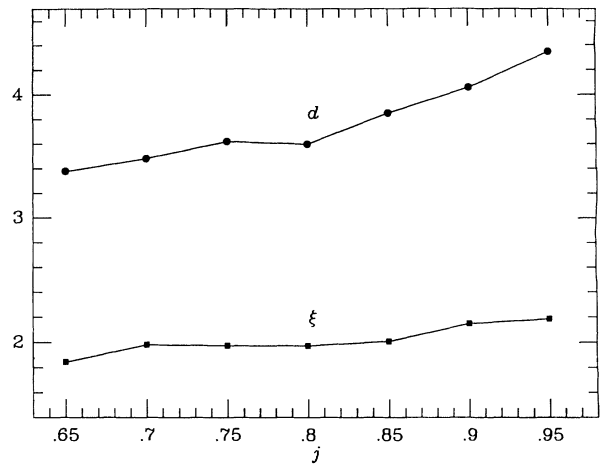

FIG. 9. Monte Carlo data for d and ξ as a function of j, with m held at a constant value of -0.11. This ray passes close to the Monte Carlo predicted Lifshitz point.

of d, we note that both theory and simulation are in quite good qualitative agreement with such experimental values of d and ξ as a function of concentration as we possess [3]. However, as of yet no serious attempt has been made to fit a sequence of data using the recursion relations (3.13) and (3.14).

Finally, it is possible to study the locus $b_r(j,m)=0$. This corresponds to the "ideal" situation where the effective renormalized "tension" is zero. This no longer corresponds to the ray $j+12m=0$, but becomes the curve in Fig. 10. The fact that such a stable condition exists for fluctuating, interacting surfaces is highly nontrivial when one views these as mechanical objects. Thus, any bare surface Hamiltonian with tensionless surface will renormalize to one that possesses a tension. This reflects the fact that the condition of zero renormalized tension and finite renormalized curvature is an unstable fixed point for a mechanical surface [11]. The same trends are evident in the present Hamiltonian since a zero bare tension becomes renormalized to a finite value. However, the Hamiltonian along $b_r(j,m)=0$ is quite stable and there is a manifold of bare values (j,m) from which it is

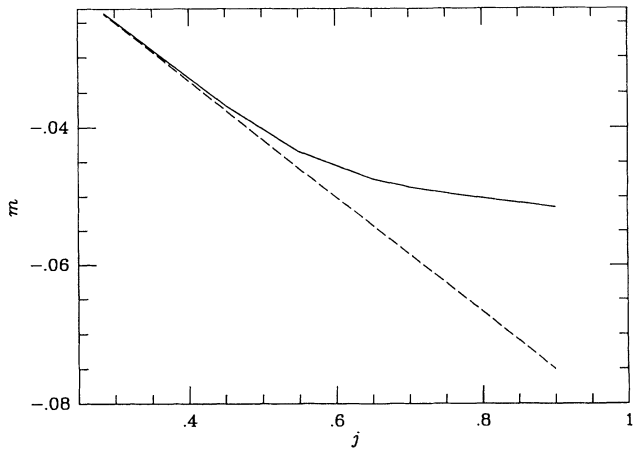

FIG. 10. Comparison of $j+12m=0$ (dashed line), and $b_r=0$ (solid line).

accessible. That nature is able to so successfully exploit this rather restricted portion of the phase-diagram reflects the fact that the bare parameters of the underlying "surface," which is open to mass exchange, can be adjusted rather delicately. Such a choice is in fact what we mean by bicontinuous microemulsion.

IV. EQUATION OF STATE

So far the approximation of the two-point function has been controlled, since it is possible to compute the renormalizations of all the couplings. However, the calculation of the equation of state within the same approximation becomes considerably more involved. We therefore introduce another approximation to the equation of state [9,10], again similar to that used by Brazovskii. It corresponds to the resummation to all orders of only the momentum independent diagrams in Fig. 1. Thus, only c will be renormalized, while b will retain its bare value. Such a procedure may be justified by the relative smallness of the shift in b predicted from Eqs. (3.13) and (3.14), but as we see later, it does have certain limitations in the regime of tensionless interfaces.

The lamellar phase is characterized by a periodically varying order parameter

$$\bar{\varphi}(\mathbf{r})=2a\cos(\mathbf{q}_c\cdot\mathbf{r}) . \tag{4.1}$$

It is also convenient to define ($b<0$)

$$G^{-1}(q_c)=c-\frac{b^2}{4}\equiv\Delta_0 \tag{4.2}$$

which is the inverse bare susceptibility in the paramagnetic phase. The corresponding renormalized quantities in the paramagnetic and lamellar phases are, respectively,

$$\Delta_P=c_P-\frac{b^2}{4} , \tag{4.3}$$

$$\Delta_L=c_L-\frac{b^2}{4} . \tag{4.4}$$

Note that here c_P and c_L are the renormalized masses in the paramagnetic and lamellar phases, and that b is unaffected by the present resummation of the momentum-independent diagrams.

The equation of state is calculated by dividing the original field into a mean ($\bar{\varphi}$) and fluctuating part (ψ), integrating over the latter and finding the derivative

$$h(\mathbf{x})=\frac{\delta F}{\delta\bar{\varphi}(\mathbf{x})}=\left\langle\frac{\delta H}{\delta\bar{\varphi}(\mathbf{x})}\,\middle|_{\psi=\text{const}}\right\rangle , \tag{4.5}$$

where F is the free energy associated with the action (2.11) and $h(x)$ may be thought of as a position-dependent magnetic field. It is then possible [9] to show that, if one includes only the momentum-independent diagrams, the equation of state is given by

$$h=\Delta_L a-\tfrac{1}{2}\lambda a^3 , \tag{4.6}$$

where the equation for renormalized inverse susceptibility in the lamellar phase is given by

$$\Delta_L=\Delta_0+\frac{\lambda}{8\pi}\frac{1}{(2\sqrt{c_L}+b)^{1/2}}+\lambda a^2 \tag{4.7}$$

while the renormalized inverse susceptibility in the paramagnetic phase satisfies

$$\Delta_P=\Delta_0+\frac{\lambda}{8\pi}\frac{1}{(2\sqrt{c_P}+b)^{1/2}} . \tag{4.8}$$

We now make an ansatz [12] that in the region of interest we can approximate

$$\Delta_{L,P}\approx-\frac{b}{2}(2\sqrt{c_{L,P}}+b) . \tag{4.9}$$

With this approximation Eqs. (4.7) and (4.8) become

$$\Delta_L=\Delta_0+\frac{\lambda\sqrt{-b}}{8\pi\sqrt{2\Delta_L}}+\lambda a^2 , \tag{4.10}$$

$$\Delta_P=\Delta_0+\frac{\lambda\sqrt{-b}}{8\pi\sqrt{2\Delta_P}} . \tag{4.11}$$

In the absence of the magnetic field Eq. (4.10) simplifies further to become

$$-\Delta_L=\Delta_0+\frac{\lambda\sqrt{-b}}{8\pi\sqrt{2\Delta_L}} . \tag{4.12}$$

Equation (4.12) has real solutions for $-\Delta_0\geq\Delta_c$. At this point a nonuniform metastable state will appear with a finite amplitude a_c and eventually evolves into the thermodynamically stable phase [9].

To find the phase-separation curve it is necessary to calculate the free-energy difference (ΔF) between the lamellar and paramagnetic phases. To achieve this we assume that the field h is no longer zero but varies uniformly across the phase boundary, commencing with $h=0$, $a=0$, and terminating with $h=0$, $a\neq0$[9]. Then,

$$\frac{\partial F}{\partial a}=\sum_{\mathbf{p}}\frac{\partial F}{\partial\bar{\varphi}_{\mathbf{p}}}\frac{\partial\bar{\varphi}_{\mathbf{p}}}{\partial a}=2h , \tag{4.13}$$

$$\Delta F=\int_0^{a_c}2h\,da=\int_0^{a_c}2\Delta a\,da-\frac{\lambda}{4}a_c^4 . \tag{4.14}$$

The integral on the right can be carried out by changing variables with the aid of Eq. (4.10) to obtain

$$\Delta F=\frac{1}{2\lambda}(\Delta_L^2-\Delta_P^2)+\frac{\sqrt{-b}}{8\pi\sqrt{2}}(\Delta_L^{1/2}-\Delta_P^{1/2})-\frac{\lambda}{4}a_c^4 . \tag{4.15}$$

Finally, making use of the equation of state (4.6) in zero field, the expression for the free energy simplifies to

$$\Delta F=-\frac{1}{2\lambda}(\Delta_L^2+\Delta_P^2)+\frac{\sqrt{-b}}{8\pi\sqrt{2}}(\Delta_L^{1/2}-\Delta_P^{1/2}) , \tag{4.16}$$

where Δ_L and Δ_P are given by Eqs. (4.11) and (4.12). To study these equations it is convenient to write them in dimensionless form. Thus, let

$$a=\frac{\sqrt{-b}}{8\pi\sqrt{2}} \tag{4.17}$$

and

$$\Delta_P = a^{2/3} x_P \ , \tag{4.18}$$

$$\Delta_L = a^{2/3} x_L \ , \tag{4.19}$$

$$\Delta_0 = a^{2/3} x_0 \ . \tag{4.20}$$

Equations (4.11) and (4.12) then become

$$-x_L = x_0 + \frac{1}{\sqrt{x_L}} \ , \tag{4.21}$$

$$x_P = x_0 + \frac{1}{\sqrt{x_P}} \ , \tag{4.22}$$

and the free energy

$$\Delta F = \frac{a^{4/3}}{\lambda} \left[\frac{-x_L^2}{2} + \sqrt{x_L} - \frac{x_p^2}{2} - \sqrt{x_p} \right] . \tag{4.23}$$

The equation can be solved numerically to show that ΔF changes sign at $x_0 = -2.030\,81$. The phase-separation line is then given by

$$c(j,m) - \frac{b(j,m)^2}{4} = -2.030\,81 \left[\frac{\lambda(j,m)\sqrt{-b(j,m)}}{8\pi\sqrt{2}} \right]^{2/3} . \tag{4.24}$$

We note that this refers only to the lamellar-disorder line because of condition (4.1). In fact, it can be shown that the Hamiltonian (2.11) produces numerous tubular and cubic phases for small values of j [5–7].

The plot of the curve (4.24) in the j,m plane is shown in Fig. 11. It is in qualitative agreement with the phase-transition line obtained from the Monte Carlo data, giving about 100% shift in critical temperature and being of the first order. However, it also possesses an additional feature that the Lifshitz point is no longer present. Instead the curve becomes asymptotic to the line $j+12m=0$. Based on our calculation of $b_r(j,m)=0$, which separates the ferromagnetic from the lamellar phase, we believe that this prediction is incorrect and rather reflects the fact that, for the paramagnetic-lamellar phase-transition curve, we have not included any momentum-dependent diagrams in the free-energy calculation. Physically this means that we have failed to permit the tension to renormalize along the transition curve. Where the bare tension b is vanishingly small this is a serious error. However, it does not effect the basic prediction that the lamellar-disordered phase boundary is a fluctuation-induced first order, nor does it affect the properties within the disordered (microemulsion) phase. Even so, this limitation does have the unfortunate consequence that the status of the Lifshitz point beyond the mean-field theory remains uncertain. Below we shall argue that, on the basis of the present calculations, it becomes a Lifshitz tricritical point. However, if at all possible the free-energy calculation should be pursued to the two-loop level.

We now turn to the curve of transitions from the ferromagnetic to the paramagnetic phases. Under renormalization this mean-field line of second-order transitions,

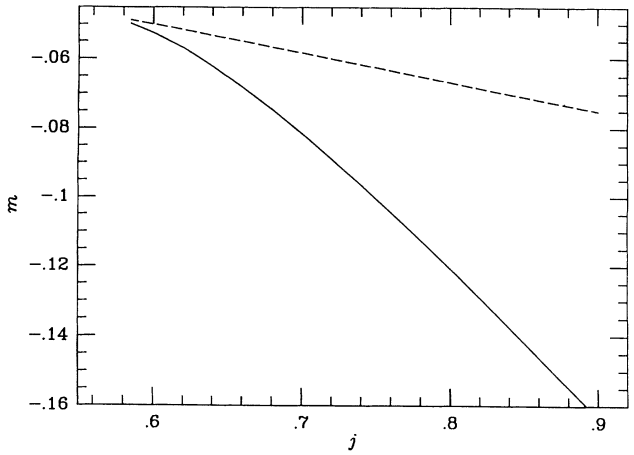

FIG. 11. Isotropic-Lamellar first-order transition line (solid line) in the j,m, parameter space as it is shown to come asymptotically close to the $j+12m=0$ line (dashed line).

$$1-6(j+5m)=0 \ , \tag{4.25}$$

remains second order and thus cannot be renormalized to arbitrary high order in the diagrammatic expansion [13]. Only the simple momentum-independent Hartree (one-loop) diagram is infrared convergent and, in fact, the high-momentum regularization is accomplished automatically by the retention of the $o(q^4)$ terms in the bare propagator, rendering a cutoff unnecessary. Thus, we can locate the new curve of second-order phase transitions by solving the equation $c_r=0$, essentially (3.14) with the λ^2 term on the right-hand side omitted. The result is presented as a curve of dots in Fig. 12.

We shall now attempt to synthesize the information from the various calculations in order to present a coherent picture of the phase diagram. Thus, we have both the renormalized ferromagnetic-paramagnetic curve to order λ and a fluctuation-induced first-order paramagnetic-lamellar curve to order λ which should, as

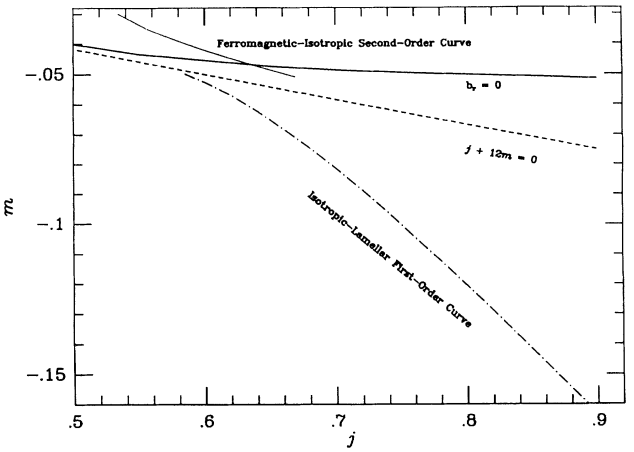

FIG. 12. The renormalized phase diagram. The $j+12m=0$ line (dashed line) is drawn for perspective. The main features are the intersection of the $c_r=0$ curve (dotted line) with the $b_r=0$ curve (solid line). This intersection point defines the predicted renormalized Lifshitz point.

in the mean-field theory, join along with the lamellar-ferromagnetic transition to form a corrected phase diagram [14]. However the problem with this procedure is evident from the examination of Fig. 12. There we see that the lamellar-ferromagnetic curve intersects the ferromagnetic-paramagnetic-transition curve, but the fluctuation-induced first-order lamellar-paramagnetic-transition curve fails to intersect either of the above. We alluded to what we believe to be one possible origin of this problem earlier in [14]. It was noted that the continuous Hamiltonian of the type (2.11) cannot contain within its phase diagram an isotropic Lifshitz point. Such a point is unstable with respect to thermal fluctuations that occur in model (2.11). However, a Lifshitz or a Lifshitz tricritical point might indeed occur in the phase diagram of a lattice Hamiltonian (1.3), since the symmetry-breaking effects of the lattice might be sufficient to stabilize it to thermal fluctuations. In this case a consistent treatment of the Lifshitz region, should, in principle, make all of these phase-separation curves join. For the continuous Hamiltonian (2.11) the most likely scenario is that thermal fluctuations prevent order from developing in the vicinity of Lifshitz point at any finite temperature, causing the paramagnetic phase to intrude between the ferromagnetic and lamellar phases. Inclusion of higher classes of diagrams might help to clarify some of these questions.

In the absence of more complete treatment it seems likely that the topology of the phase diagram implied by the present calculation for model (1.3) is still correct. In that case the intersection of the renormalized ferromagnetic-paramagnetic and disorder curves is the location of the new Lifshitz tricritical point. That it should be a tricritical point is evident from the fact that it will simultaneously be the terminus of the curve of fluctuation-induced paramagnetic-lamellar phase transitions and the beginning of a curve of second-order ferromagnetic-paramagnetic transitions. These remarks have been represented in the sketch of the proposed renormalized phase diagram, Fig. 12. We emphasize, however, that the precise nature of the Lifshitz region of the lamellar-paramagnetic curve still remains an open question.

V. CONCLUSIONS

In summary then, we point out that starting with a lattice-model Hamiltonian, we have extracted a Landau theory with bare parametric dependences. This theory can be quantitatively renormalized to produce the renormalized transition lines and correlation functions of the theory. These are in fair agreement with the Monte Carlo data, in contrast to the erroneous predictions of the mean-field theory. We have established that a tension-free renormalized Hamiltonian is quite accessible to a range of the bare parameter b, and conclude that the large-swelling limit of bicontinuous microemulsion should be, in principal, accessible to experiment.

Each segment of the renormalized phase diagram seems fairly satisfactory; the qualitative and sometimes quantitative agreement with Monte Carlo is established, strengthening the sometimes difficult interpretations of the latter. The major weakness remains the lack of any effective Hamiltonian that can carry one across the Lifshitz region precisely at the order-disorder transition.

ACKNOWLEDGMENTS

This work was supported by Grant No. 21718-G6 from the American Chemical Society Petroleum Research Fund and a fellowship from the David and Lucille Packard Foundation.

APPENDIX A

The ansatz of Sec. IV is not necessary. In fact the equations can be solved numerically. However, this is considerably more difficult and the closed form for the phase transition line (4.24) is no longer obtainable. Of course the final justification of this ansatz is that it indeed gives the same phase-transition curve as the full numerical solution. In this appendix we carry out this calculation.

Using the exact procedure outlined in Sec. IV, except for the ansatz, the self-consistent equations (4.12) and (4.11) become, respectively,

$$-c_L=-\frac{b^2}{2}+c+\frac{\lambda}{8\pi(2\sqrt{c_L}+b)^{1/2}}\ , \tag{A1}$$

$$c_P=c+\frac{\lambda}{8\pi(2\sqrt{c_P}+b)^{1/2}}\ . \tag{A2}$$

Starting with Eqs. (4.6) and (4.13), the equation for the change in free energy becomes

$$\begin{aligned}\Delta F=&-\left[\frac{c_L^2}{2\lambda}+\frac{c_P^2}{2\lambda}\right]\\&+\frac{1}{16\lambda}b^4\{\tfrac{2}{3}[(2\sqrt{c_L}+b)^{3/2}-(2\sqrt{c_P}+b)^{3/2}]\\&-\frac{1}{64\pi}4b[(2\sqrt{c_L}+b)^{1/2}-(2\sqrt{c_P}+b)^{1/2}]\\&-2b^2[(2\sqrt{c_L}+b)^{-1/2}-(2\sqrt{c_P}+b)^{-1/2}]\}\ .\end{aligned} \tag{A3}$$

The values of b, c, and λ as a function of j, and m are given by Eqs. (2.12)–(2.14). For a fixed value of j, a value for the microscopic parameter m is found that satisfies the equation $\Delta F=0$ and the constraints (A1) and (A2). The resulting line of first-order transitions is shown in Fig. 13 and compared to the curve of first-order transitions resulting from the ansatz. The two are in excellent agreement.

APPENDIX B

Higher-order momentum-dependent diagrams will contribute to Eq. (3.4) and the next one is shown in Fig. 1. The expression for the last diagram on the right is

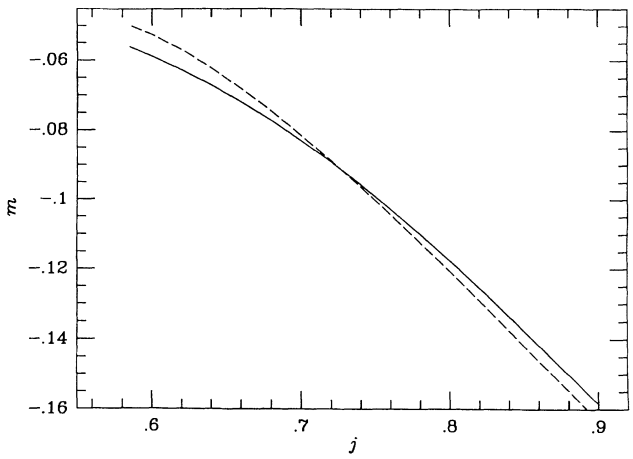

FIG. 13. Comparison of the closed-form isotropic-lamellar first-order transition line obtained from the ansatz (dashed line) and that obtained from the methods in Appendix A (solid line).

$$I=\left[\frac{1}{(2\pi)^3}\right]^3\int G(\mathbf{k}_1)G(\mathbf{k}_2)G(\mathbf{k}_3)G(\mathbf{q}-\mathbf{k}_2-\mathbf{k}_1)\times G(\mathbf{k}_1+\mathbf{k}_2-\mathbf{k}_3)d^3\mathbf{k}_1 d^3\mathbf{k}_2 d^3\mathbf{k}_3 \ . \tag{B1}$$

Once again by changing to real space we can estimate the bound on this integral. We find that $I\approx(4\pi)^2cK^5\xi$, where c is a numerical factor of order 0.1. Since K and ξ are large only in the vicinity of the second-order phase transition, which has been shifted to zero temperature in the present analysis, one would expect the expansion to be controlled by these factors. The true situation is, however, more subtle. Consider for example the contribution to self-energy arising from Eq. (B1). It would seem reasonable to estimate its contribution by using the renormalized values of the coupling constants from the calculations in the previous order. When one performs this estimate the contribution is quite large (mainly because λ^3 is large). However, this procedure is not valid due to the strong nonlinearity of the self-consistent equation for self-energy. Thus, even though the individual terms of the equation are large the final contribution to the renormalization of the couplings is not nearly as great. We can demonstrate this by estimating the contribution to mass renormalization coming from the two-loop integral. In fact, since we have the two-loop renormalized answer we can compare it to the estimate. The true two-loop contribution to mass renormalization beyond the Hartree level (one loop) is fairly small ($c_{\text{bare}}=-12.1$, $c_H=2.76$, $c_{\text{two loop}}=4.9$), while the procedure outlined above would overestimate the value of the renormalized mass by 300% (for a sample point $j=0.6$, $m=-0.06$). We therefore have reason to suppose that the failure of the naive argument does not represent the failure of the low-order series (3.4) to well represent fluctuations. However, at the moment we have no more rigorous bound on the higher-order terms.

Finally, as a check on the validity of φ^4 theory perturbation rather than the full nonlinearity for the Hubbard transformation we have solved the full gap equation for the complete nonlinear potential at one-loop order. This calculation was carried out for the ferromagnetic-paramagnetic boundary near the problematic Lifshitz region. The difference between the φ^4 and full nonlinear theory is small. Such a calculation for the lamellar-paramagnetic boundary is more involved and we have not accomplished it yet.

APPENDIX C

The correlation function for solvent and lipid scattering within the microemulsion (disordered) region are given, respectively, in Ising model language by [5,15]

$$\langle\delta\rho_{\mathbf{n}}^{AA}\delta\rho_{\mathbf{n}'}^{AA}\rangle=\tfrac{1}{4}\langle\sigma_{\mathbf{n}}\sigma_{\mathbf{n}'}\rangle \ , \tag{C1}$$

$$\langle\delta\rho_{\mathbf{n}}^{AB}\delta\rho_{\mathbf{n}'}^{AB}\rangle=\frac{1}{4}\left[\sum_{\hat{\mathbf{a}}}\langle\sigma_{\mathbf{n}}\sigma_{\mathbf{n}+\hat{\mathbf{a}}}\sigma_{\mathbf{n}'}\sigma_{\mathbf{n}'+\hat{\mathbf{a}}}\rangle-\langle\sigma_{\mathbf{n}}\sigma_{\mathbf{n}+\hat{\mathbf{a}}}\rangle\langle\sigma_{\mathbf{n}'}\sigma_{n'+\hat{\mathbf{a}}}\rangle\right] , \tag{C2}$$

where $\sigma_{\mathbf{n}}$ is the Ising spin variable which may take the values ±1, and the index $\hat{\mathbf{a}}$ denotes a unit vector between nearest neighbors, ρ^{AA} denotes the density of a solvent species (water or oil), and ρ^{AB} denotes the density of the lipid. The Gaussian approximation to the solvent-solvent correlation function is given by Eqs. (3.7)–(3.10). Finally, for completeness, we present the Gaussian approximation to the scattering of Eq. (C.2):

$$S(q)=\frac{g^2(0)\pi}{q\beta^2}\left[\tan^{-1}\left[\frac{q}{2\alpha}\right]+\tan^{-1}\left[\frac{2\beta-q}{2\alpha}\right]-\tan^{-1}\left[\frac{2\beta+q}{2\alpha}\right]\right] , \tag{C3}$$

where $\alpha=1/\xi$ and $\beta=2\pi/d$. Certainly there will be strong renormalization of the above scattering function, just as there was for the solvent scattering. We note that inclusion of a quartic field term in calculating the average in Eq. (C2) would require the renormalization of the four-point vertex function. In any case, it is not entirely clear if a continuum field theory is satisfactory to represent the short-distance behavior implied by Eq. (C2).

[1] W. Selke, Z. Phys. B **27**, 81 (1977); P. Bak and J. von Boehm, Phys. Rev. B **21**, 5297 (1980); M. E. Fisher and W. Selke, Philos. Trans. R. Soc. London **302**, 1 (1981); C. S. O. Yokoi, M. D. Coutinho-Filho, and S. R. Salinas, Phys. Rev. B **24**, 4047 (1981); W. Selke and J. M. Yeomans, Z. Phys. B **46**, 211 (1982); P. Bak, Rep. Prog. Phys. **45**, 587 (1982); W. Selke, K. Binder, and W. Kinzel, Surf. Sci. **125**, 74 (1982); W. Selke and P. M. Duxbury, Z. Phys. B **57**, 49 (1984); A. Aharony, E. Domany, R. M. Hornreich, T. Schneider, and M. Zannetti, Phys. Rev. B **32**, 3358 (1985);

P. Upton and J. Yeomans, *ibid.*, **40**, 479 (1989); M. C. Barbosa, *ibid.* **42**, 6363 (1990); M. C. Barbosa (unpublished).

[2] B. Widom, J. Chem. Phys. **84**, 6943 (1986).

[3] S. A. Chen, S. L. Chang, R. Strey, J. Samseth, and K. Mortensen (unpublished); S.-H. Chen, S.-L. Chang, and R. Strey, J. Chem. Phys. **93**, 1907 (1990); E. W. Kaler, K. E. Bennett, H. T. Davis, and L. E. Scriven, *ibid.* **79**, 5673 (1983); H. Saito and K. Shinoda, J. Colloid Interface Sci. **102**, 647 (1970); C. Cabos and P. Delord, J. Appl. Cryst. **12**, 502 (1979); M. Kolarchyk, S.-H. Chen, J. S. Huang, and M. W. Kim, Phys. Rev. A **29**, 2054 (1984); M. Kolarchyk, S.-H. Chen, J. S. Huang, and M. W. Kim, Phys. Rev. Lett. **53**, 941 (1984); B. H. Robinson, C. T. Toprakcioglu, J. C. Dore, and P. Chieux, J. Chem. Soc. Faraday Trans. 1 **80**, 13 (1984); S.-H. Chen, T. Lin, and J. S. Huang, in *Physics of Complex Supermolecular Fluids, Exxon Monograph,* edited by S. A. Safran and N. A. Clark (Wiley, New York, 1987).

[4] M. Teubner and R. Strey, J. Chem. Phys. **87**, 3195 (1987).

[5] K. A. Dawson, M. D. Lipkin, and B. Widom, J. Chem. Phys. **88**, 5149 (1988); K. A. Dawson, Phys. Rev. A **36**, 3383 (1987).

[6] K. A. Dawson and C. J. Mundy, *Inhomogeneous Fluids,* edited by D. Henderson (Marcel Dekker, NY, 1992); G. Gompper, R. Holyst, and M. Schick, Phys. Rev. A **43**, 3157 (1991); G. Gompper and M. Schick, Phys. Rev. Lett. **65**, 1116 (1990).

[7] K. A. Dawson, B. L. Walker, and A. Berera, Physica A **165**, 320 (1990).

[8] Y. Levin and K. A. Dawson, Phys. Rev. A **42**, 1977 (1990).

[9] S. A. Brazovskii, Zh. Eksp. Teor. Fiz. **68**, 175 (1975) [Sov. Phys. JETP **41**, 85 (1975)].

[10] G. H. Fredrickson and E. Helfand, J. Chem. Phys. **87**, 697 (1987).

[11] L. Peliti and S. Leibler, Phys. Rev. Lett. **54**, 1690 (1985).

[12] This can be justified by the fact that in the region of interest $2\sqrt{c_r} \approx -b$, as can be seen by explicitly solving Eq. (4.8). The ansatz allows us to express the first-order transition line in a closed form. Of course it is not necessary and the calculation can be carried out numerically (see Appendix A).

[13] Beyond the Hartree approximation there is no simple perturbative correction and one must return to the renormalization group. It is also interesting to note that in the present theory retention of the $O(q^4)$ term renders the theory ultraviolet convergent removes the necessity for a large-momentum cutoff [see G. Parisi, *Statistical Field Theory* (Addison-Wesley, Redwood City, 1988), Chap. 6].

[14] At this point one should perhaps draw a distinction between the lattice model, as a representation of, for example, magnetic order on a lattice and amphiphilic mixtures. The details at the Lifshitz point may be different in these situations. Thus, the lattice umklapp terms are known to be relevant at the Lifshitz point, inducing order that would not be present in the continuum theory. This issue is discussed in Y. Levin and K. A. Dawson, Phys. Rev. A **42**, 3507 (1990); and Y. Levin, Phys. Rev. B **43**, 10 876 (1991). The Hamiltonian (2.11) is not valid precisely at a putative Lifshitz point in three dimensions.

[15] K. A. Dawson, Phys. Rev. A **35**, 1766 (1987).